

Obstructed Surface States as the Descriptor for Predicting Catalytic Active Sites in Inorganic Crystalline Materials

Guowei Li,* Yuanfeng Xu, Zhida Song, Qun Yang, Yudi Zhang, Jian Liu, Uttam Gupta, Vicky Süß, Yan Sun, Paolo Sessi, Stuart S. P. Parkin, B. Andrei Bernevig,* and Claudia Felser*

The discovery of new catalysts that are efficient and sustainable is a major research endeavor for many industrial chemical processes. This requires an understanding and determination of the catalytic origins, which remains a challenge. Here, a novel method to identify the position of active sites based on searching for crystalline symmetry-protected obstructed atomic insulators (OAI) that have metallic surface states is described. The obstructed Wannier charge centers (OWCCs) in OAI are pinned by symmetries at some empty Wyckoff positions so that surfaces that accommodate these sites are guaranteed to have metallic obstructed surface states (OSSs). It is proposed and confirmed that the OSSs are the catalytic activity origins for crystalline materials. The theory on 2H-MoTe₂, 1T'-MoTe₂, and NiPS₃ bulk single crystals is verified, whose active sites are consistent with the calculations. Most importantly, several high-efficiency catalysts are successfully identified just by considering the number of OWCCs and the symmetry. Using the real-space-invariant theory applied to a database of 34 013 topologically trivial insulators, 1788 unique OAI are identified, of which 465 are potential high-performance catalysts. The new methodology will facilitate and accelerate the discovery of new catalysts for a wide range of heterogeneous redox reactions.

for the design of highly active catalysts is the identification of the origin of the activity. However, this remains a challenge.^[8,9] The activity of a given catalyst is traditionally associated with the properties of its surfaces. Thus, materials with large surface areas, good conductivity, and high mobility are understood to be good catalysts, as they have abundant active sites that favor the adsorption of intermediates and electron transfer in redox reactions. This is the motivation for widely used catalyst synthesis strategies such as nanostructuring, doping, alloying, or adding defects. Each method aims to either expose preferential crystal surfaces or engineer them to make them more active.^[10–12] However, it is still a formidable task to locate the position of active sites rapidly and precisely from the design perspective, making the discovery of high-performance catalysts from the many potentially interesting materials a challenge.


1. Introduction

High-performance heterogeneous catalysts are key to the preparation of many chemicals that are the foundation of, amongst others, photo- and electrochemical water splitting,^[1–5] fuel cells, hydrogenation, and the Haber–Bosch process.^[6,7] A prerequisite

for topological materials have robust surface states and massless electrons with high mobilities.^[13–15] Moreover, many state-of-the-art catalysts (such as Pt, Pd, Cu, Au, IrO₂, and RuO₂) are understood, either from theory or experiment, to have topologically derived surface states (TSSs).^[16,17] Thus, there is some evidence for the important role of TSSs in catalytic reactions.^[18,19] Such states are mainly composed of

G. Li, Y. Zhang, J. Liu
CAS Key Laboratory of Magnetic Materials and Devices
and Zhejiang Province Key Laboratory of Magnetic Materials and
Application Technology
Ningbo Institute of Materials Technology and Engineering
Chinese Academy of Sciences
Ningbo 315201, China
E-mail: liguowei@nimte.ac.cn

G. Li, Y. Zhang, J. Liu
University of Chinese Academy of Sciences
Shijingshan District, Beijing 100049, China

 The ORCID identification number(s) for the author(s) of this article can be found under <https://doi.org/10.1002/adma.202201328>.

© 2022 The Authors. Advanced Materials published by Wiley-VCH GmbH. This is an open access article under the terms of the Creative Commons Attribution License, which permits use, distribution and reproduction in any medium, provided the original work is properly cited.

G. Li, Q. Yang, U. Gupta, V. Süß, Y. Sun, C. Felser
Max Planck Institute for Chemical Physics of Solids
01069 Dresden, Germany
E-mail: guowei.li@cpfs.mpg.de; Claudia.Felser@cpfs.mpg.de

Y. Xu, P. Sessi, S. S. P. Parkin, B. A. Bernevig
Max Planck Institute of Microstructure Physics
06120 Halle (Saale), Germany

Z. Song, B. A. Bernevig
Department of Physics
Princeton University
Princeton, NJ 08544, USA
E-mail: bernevig@Princeton.EDU

B. A. Bernevig
Donostia International Physics Center
P. Manuel de Lardizabal 4, Donostia-San Sebastian 20018, Spain

DOI: 10.1002/adma.202201328

highly delocalized *sp*-orbitals (noble metals) or *d* orbitals with strong spin-orbit coupling (noble metal oxides). Furthermore, these states are fundamentally derived from the band structure of the bulk material, and, thus, must be distinguished from what one might term “topologically trivial” surface modifications that form the basis of many of the common strategies to increase catalytic activity, mentioned above.^[20,21]

In this work, we propose that the obstructed surface states (OSSs) of OAIs form a new class of active sites for inorganic heterogeneous catalysts. Like TSSs, the OSSs originate from the topologies of bulk electronic bands and provide open sites for molecular adsorption. The OSSs can exist in clean, large-gap, topologically trivial insulators and are separated from the bulk states in the energy spectrum, unlike TSSs, which are always connected to bulk states with a small bandgap. Using the topological quantum chemistry (TQC) theory and the RSIs developed in our previous works,^[6–9] we have identified 1788 unique OAIs (3383 Inorganic Crystal Structure Database entries),^[26] of which 465 unique compounds have promising catalytic activities. Most importantly, we also predict their Miller indices of specific cleaved surfaces which have active sites. Thus, our work gives a clear direction for both the

understanding and the design of high-performance catalysts from the numerous known inorganic compounds.

2. Results and Discussion

We address this problem by taking both the bulk electronic structure and the crystal geometry into consideration. As schematically shown in **Figure 1A**, for all the compounds with crystal structures provided in the Inorganic Crystal Structure Database (FIZ Karlsruhe, Germany),^[27] we have calculated their electronic structures and symmetry eigenvalues with the data now available to the public via the Topological Materials Database,^[23a] where all the materials are classified into trivial and topological materials (insulators, semimetals, metals). In the next step, for all the band representations of topologically trivial insulators, we calculate their 3D real space invariants (RSIs),^[22,23,26] which characterize the multiplicities of symmetric Wannier functions pinned at the real-space positions that are referred to as the obstructed Wannier charge centers (OWCCs).^[26] Finally, we have provided the Miller indices of cleavage planes that cut through the OWCCs and lead to the metallic OSSs.

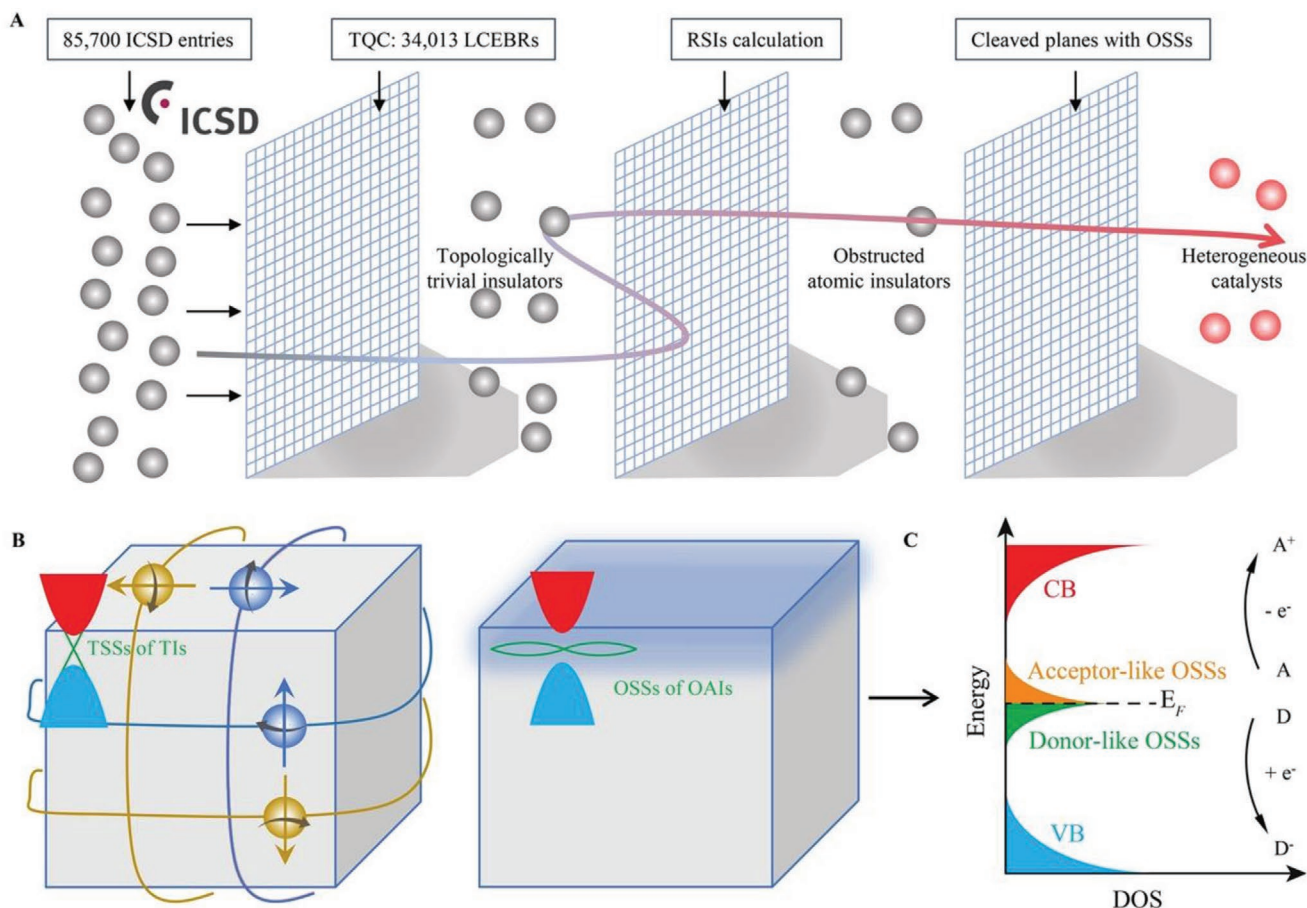


Figure 1. The design of heterogeneous catalysts from obstructed atomic insulators (OAIs). A) Screening of potential OAIs and heterogeneous catalysts from the Topological Materials Database website (see ref. [23a]) by calculating the RSIs. B) Comparisons between the TSSs and OSSs. C) Illustration of the role of OSSs in OAIs for reduction and oxidation catalytic reactions.

The usual dangling bond can be thought of as the simplest case of OSSs, where the OWCC resides between two bonding atoms and the OSSs at the surface are just the broken bonds and will be localized around the bonding atoms. However, the general structures of OSSs can be exotic and very different from simple dangling bonds. OSSs are distinguished from TSSs by the fact that their surface states do not fill the entire energy gap between the conduction and the valence band (Figure 1B). Thus, the crystal surface with OSSs is characterized by high conductivity, open sites for bonding and adsorption, and a high density of electronic states around the Fermi level. Therefore, the OSSs provide a straightforward path to determine the position of active sites and to guide the design of highly active catalysts by choosing desired crystal surfaces (Figure 1C). Using the RSI indices which, given a band structure, immediately determine the position of the OWCCs, we have discovered 1788 unique OAIs (3383 ICSDs), and 465 of them as potential catalysts with well-defined catalytic active sites. In this work, several representative single crystals, OAI 2H-MoTe₂, topological semimetal 1T'-MoTe₂, and OAI NiPS₃ are chosen for the experimental validation of the hypothesis. Most importantly, high-performance catalysts are predicted successfully by condensing the location and density of OSSs, including the OAIs RuP₄ and FeP₄. This work provides a descriptor to find the active sites of a given catalyst rapidly, making the design of highly active catalysts more efficient.

2.1. Results

The van der Waals compounds including 2H-MoS₂, 2H-WSe₂, and 2H-MoTe₂ [ICSD 105091, SG (Space Group) 194 (*P63/mmc*)] have been the subject of extensive research studies because of their high intrinsic catalytic efficiency for industrial-scale catalysis reactions such as hydro-desulfurization and hydrogen evolution reaction (HER).^[28–30] Electrocatalytic activity measurements on various 2H phase nanostructured catalysts have confirmed that only the edge surfaces are catalytically active toward HER, while the thermodynamically stable (001) surface has no such activity. Only when the basal surfaces are modified by defect engineering such as by making vacancies, can they be activated and optimized for catalysis because of the appearance of surface states.^[31,32] In Figure 2A, the crystal structure of 2H-MoTe₂ and the position of OWCCs are displayed. The center of charge is localized at the 2*b* position, which has no atom occupation (Tables S1 and S2, Supporting Information). This is confirmed by our surface states calculation on the (100) edge surface and (001) basal surface, as shown in Figure 2B,C. The OSSs only exist at the (100) edge surface and are located close to the Fermi level. As an HER catalyst, we predict that only the metallic edge surfaces of the 2H-MoTe₂ are catalytically active for hydrogen production.

It is an interesting question to ask can we directly see the high conductivity at the edges with OSSs. Conductive atomic force microscopy (C-AFM) could be a good choice for

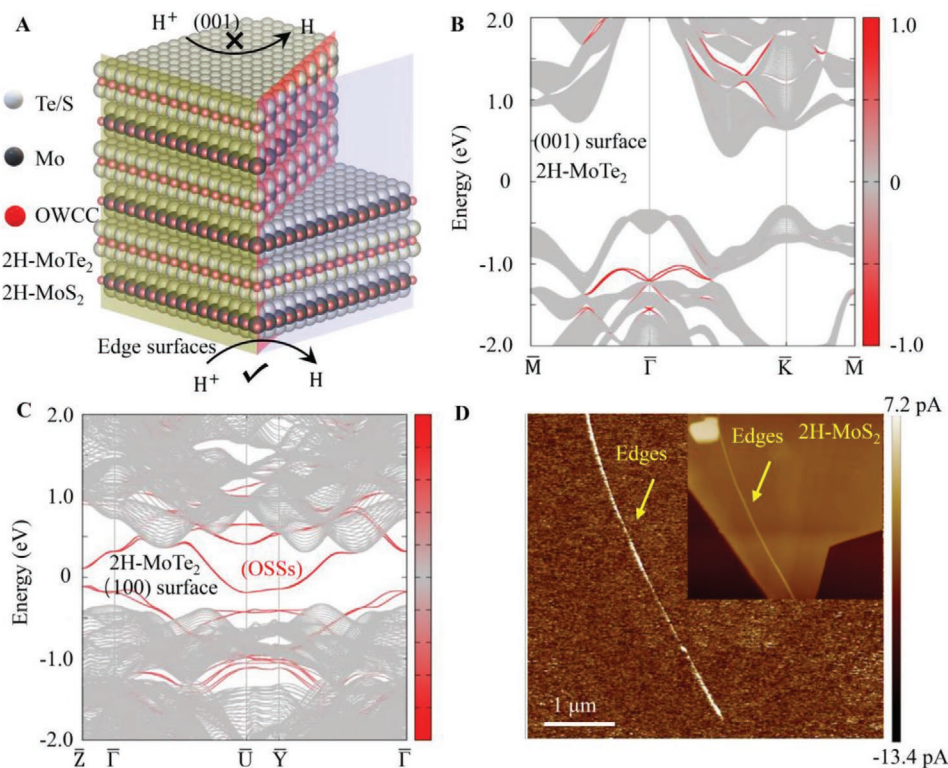


Figure 2. The relationship between OWCCs and active sites in 2H-MoTe₂ for hydrogen evolution. A) The crystal structure of 2H-MoTe₂/2H-MoS₂ and the position of OWCCs. As an HER catalyst, the (001) basal plane is catalytically inert. All the edge surfaces are active toward hydrogen evolution. The obstructed surface states calculation of 2H-MoTe₂ at the (001) (B) and (100) (C) surfaces, respectively. The OSSs only exist at the edge surfaces, such as the (100) surface. The gray and red lines represent the respective bulk and surface bands. D) C-AFM measurements across the edges and basal planes of an exfoliated MoS₂ nanoflake on an Au-coated Si substrate, suggesting the better conductivity at the edges. The inset shows the 2D mapping of the surface high-profile on one nanoflake.

conductivity mapping. This requires a high-quality sample that exposes both the edges and basal plane at the same time, which is difficult for the 2H-MoTe₂ structure. We found that 2H-MoS₂ is also an OAI with the OWCCs located at the same place as 2H-MoTe₂ (Appendix A and Figure S1a, Supporting Information). Most importantly, they have the same catalytic behaviors toward HER, with only the edges being catalytically active (Figure S1b, Supporting Information).^[33] Nanoflakes with different thicknesses were mechanically exfoliated from the bulk single crystal with different tape and methods (Figure S1c–e, Supporting Information). C-AFM on the whole crystal surface confirmed that the conductivity at the edges is much better than the basal plane (Figure 2D, Figure S1e, Supporting Information) confirming the existence of metallic electronic states at the measurement edges.

To confirm this prediction, we synthesized high-quality 2H-phase and 1T'-phase of MoTe₂ bulk crystals, respectively.^[34] The size of the investigated 2H-phase MoTe₂ crystal is 3 × 5 × 1 mm³, with the basal plane determined to be the (001) plane by the Laue diffraction technique (Figure S2, Supporting Information). Thus, the edge surfaces and basal (001) surfaces can be distinguished easily with the naked eye. The single crystal was then attached to a Ti wire and served as the working electrode. To obtain the surface dependent HER behaviors of the 2H phase single crystal, we first measured the linear sweep voltammetry (LSV) curve of the whole crystal. The edge surfaces and basal (001) surface were then covered by gel, thus we can determine the contribution from the (001) surface and edge surfaces, respectively. LSV curves indicate that the activity of the edge surfaces is the same as the whole crystal and much larger than that for the (001) basal surface (Figure 2B). The HER currents were also scaled with geometric surface areas. The onset potentials (defined when the current density reaches 1 mA cm⁻²) were determined to be 374, 398, and ~480 mV for the whole crystal, edges surfaces, and basal planes, respectively (Figure S3, Supporting Information). These data indicate that the catalytic activities of 2H-MoTe₂ originated from their edge surfaces. A photo of the crystal was taken during the chronopotentiometry measurements. It can be seen clearly that the hydrogen bubbles are produced only at the edge surfaces (Figure 2C). When the large basal plane was covered by gel, one can still see the hydrogen evolution at the edge surfaces (Figure S4, Supporting Information), which is consistent with the LSV results. Electrochemical impedance measurements were carried out on the whole crystal, the edge surfaces, and the basal surface (Figure 2D). The corresponding fitted Nyquist plots suggest that the edge surface (589 Ω) has a much smaller charge transfer resistance than the basal surface (646 Ω), indicating a much higher conductivity at the edge surfaces. The experimentally observed catalytic behavior of 2H-MoTe₂ is in perfect agreement with our theoretical concept.

Most van der Waals compounds expose their thermodynamically stable basal planes, which have no charge density for bonding and charge transfer with adsorbed molecules and are thus catalytically inert according to our theory. Based on our RSI calculations of the OAIs, we predict, however, that there is a class of van der Waals compounds that have surface states in their basal planes. The topological Weyl semi-metal, the 1T' phase of MoX₂ (X = S, Se, Te), which is obtained by breaking

the inversion structural symmetry of 2H-MoTe₂, is a good candidate for testing our hypothesis.^[35] In both polytypes, the Mo atoms are located at the center of a framework defined by two Te atom triangles to form an [MoTe₆] octahedral unit. In the 2H-MoTe₂ phase, the [MoTe₆] units have a trigonal prismatic structure whereas in the 1T' phase these units form distorted octahedra. This results in a charge density and metallic surface states on both (001) and (100) surfaces in the latter 1T' structure (Figure S5, Supporting Information).^[36] We synthesized high-quality 1T'-MoTe₂ single-crystals with megascopic (001) basal plane (2 × 5 × 0.2 mm³) that we confirmed with the Laue diffraction technique and Raman spectroscopy (Figures S2c and S6, Supporting Information). Indeed, HER measurements on the edges and basal planes of a bulk 1T'-MoTe₂ single-crystal confirm the prediction of our OSS theory that all the crystal surfaces are active for hydrogen production (Figure 3C). In addition, we observed a significantly lower charge transfer resistance for the (001) basal plane (89.9 Ω) than the edge surfaces (157 Ω), suggesting a high conductivity at the basal plane (Figure 3D). With this principle in mind, it is possible to determine the catalytic active surfaces of a given catalyst quickly. This can be confirmed by quasi-2D antiferromagnet NiPS₃, whose catalytic behaviors have been well documented either theoretically or with exfoliated nanoflakes from bulk singles.^[37] NiPS₃ crystallizes in the symmetries of the SG 12 (C₂/m). Thus, side surfaces that are perpendicular to the (001) surface should be equipped with the metallic surface states and be catalytically active toward the HER. Bulk single crystals of NiPS₃ in the size of 5 × 2.5 × 0.2 mm³ were synthesized with a chemical vapor transport method. LSV curves indicate that the HER activities of the whole crystal are almost contributed only by the edge surfaces when we cover the basal plane with gel (Figure S7a, Supporting Information). At the same time, hydrogen bubbles are only produced at the edge surfaces, rather than the big basal (001) plane.^[37] In agreement with the theoretical predictions, we observed an increased conductivity at selected edges on the exfoliated NiPS₃ flake using conductive Atomic Force Microscopy (AFM), supporting the existence of metallic electronic states (Figure S7b–d, Supporting Information).

New catalysts with high efficiencies can now be quickly predicted by identifying the position of the OSSs. The objective is to identify materials that have high numbers of OWCCs on a given crystal facet plus as many of these facets, as possible. The family of 3d and 4d transition metal tetra-phosphides MP₄ (M = Fe, Ru, Mn...) is a promising choice to meet this objective, and some of them contain naturally abundant and, therefore, low-cost elements. Our theory suggests that the surfaces that cut the 2d position but without overlapping with the atoms have surface states (Tables S3 and S4, Supporting Information). This indicates that the OWCCs are located between the P–P bonds as shown in the (010) surface (up Figure 4A), which means that all crystal surfaces with broken P–P bonds possess OSSs and should be catalytically active. This includes, but is not limited to the surfaces, (001), (010), and (011). It should be noted here that one cannot simply claim that the crystal with OSSs will exhibit high catalytic activities. The OSSs only guarantee that the crystal surface could be active for molecules bonding and adsorption, which means that the adsorption energy could be too strong or too weak. The classic d band theory based on

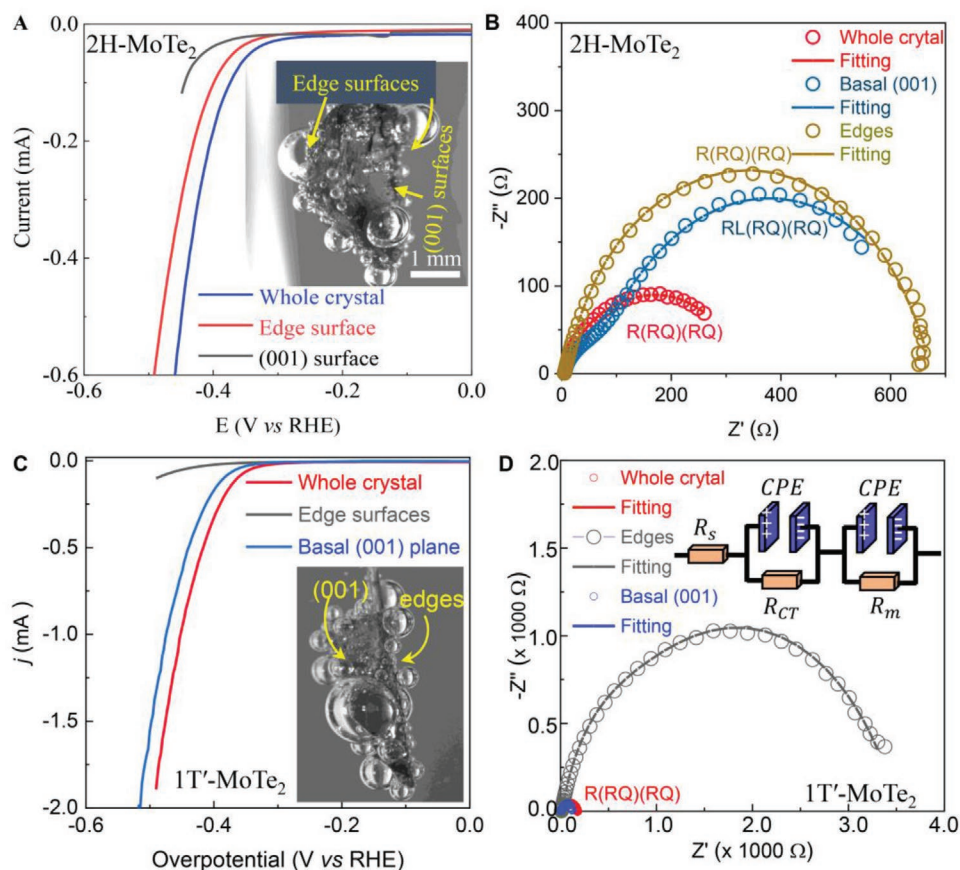


Figure 3. Experimental verification of catalytic active sites in 2H-MoTe₂ and 1T'-MoTe₂ bulk crystals. A) LSVs of the 2H-MoTe₂ HER catalyst. It can be seen clearly that almost all the activity originates from the edge surfaces. A photo of the 2H-MoTe₂ bulk single crystal during the hydrogen evolution process (with a constant overpotential of -0.43 V versus RHE) is shown as an inset. Hydrogen bubbles are observed at the edge surfaces, while the basal (001) surface is not active for hydrogen production. B) Corresponding EIS spectra that recording at different surfaces. C) Polarization curves of 1T'-MoTe₂ bulk crystal for the whole crystal, the basal (001) plane, and the edge surfaces. It can be seen that the HER activities are contributed almost entirely by the (001) basal plane. The inset confirms that the hydrogen bubbles are produced at the (001) plane. D) EIS spectra and the corresponding fitting of the 1T'-MoTe₂ bulk crystal recorded at different surfaces. One can see a much smaller charge transfer resistance when exposing the metallic (001) surface.

Sabtier's principle should be taken into consideration when one tries to understand their intrinsic activities. With this in mind, we investigated the hydrogen adsorption behavior by calculating the Gibbs free energy for hydrogen adsorption (ΔG_{H}) on the (010) surfaces. The ΔG_{H} value is 0.29 eV for the Ru sites. In contrast, this value is 0.15 eV for the P sites, which is close to that of Pt. We did the same calculation on the (001) and (011) surfaces. The ΔG_{H} values are determined to be 0.18, and 0.17 eV, respectively, which is close to the state-of-the-art Pt (111) surface (0.12 eV) (Figure S8, Supporting Information).^[38] Interestingly, we found the position of adsorbed H atom and the OWCCs are almost overlapped. This indicates that the electronic states in the OSSs should be responsible for the bond formation and preferred H adsorption energy. Considering the high density of active sites and the thermodynamically favored Gibbs free energy for hydrogen adsorption, RuP₄ should be an ideal catalyst for HER. To prove this hypothesis, we grew nanostructured RuP₄ on the Ni foam to increase the density of active sites (Figures S9 and S10, Supporting Information). The activity contribution from Ni foams can be neglected because of its high overpotentials under the same measurement condition, which is 332 mV in 0.5 M H₂SO₄, and 279 mV in 1 M KOH

(Figure 4b and Figure S11, Supporting Information).^[39] The overpotentials required to produce cathodic current densities of 10 mA cm⁻² are 28 and 31 mV using 0.5 M H₂SO₄ and 1 M KOH electrolytes, respectively, which are comparable to one of the best performing catalysts, Pt/C (Figure 4B, Figure S12, Supporting Information). Although other ruthenium phosphide phases such as RuP and RuP₂ have been reported to be excellent HER catalysts,^[40,41] we can still exclude their contribution because of the low contents and the unique synthesis strategy. The turnover frequency (TOF) of the HER using RuP₄ as the catalyst was determined by normalizing the kinetic current to the electrochemically active surface area (Figures S13 and S14, Supporting Information, Supporting Information). At an overpotential of 100 mV, the TOFs were measured to be 1.86 and 7.8 H₂ s⁻¹ in alkaline and acidic electrolytes, respectively. These values are comparable to those reported for state-of-the-art catalysts such as Pt/C (Figure 4C).^[40,42-46] In addition, the RuP₄ nanostructures exhibited good electrochemical stability as an HER catalyst, without significant activity loss during a 25 h measurement (Figure S15, Supporting Information).

Having identified RuP₄ as a high-performing catalyst we considered other members of this family containing only highly

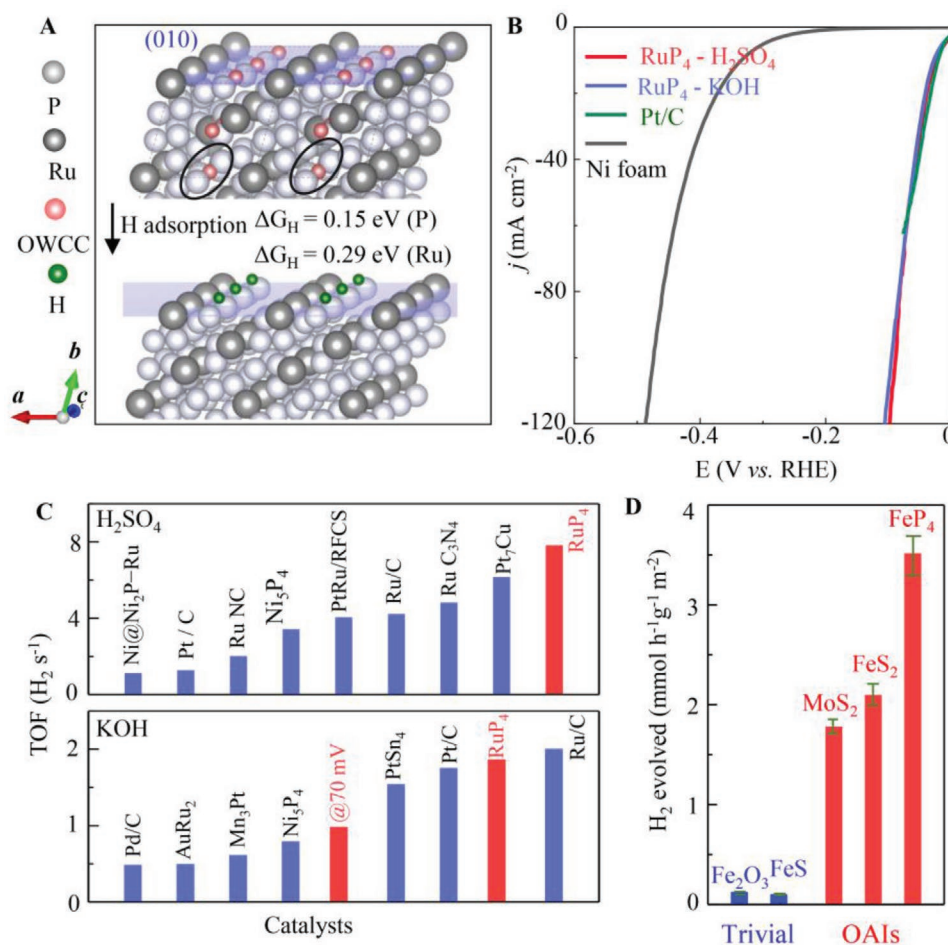


Figure 4. Prediction of high-performance HER catalysts from calculations of OSSs. A) The position of OWCCs and cleavage plane (010) gives rise to OSSs in RuP₄. The lower figure represents the H adsorption structure at the (010) surface. It can be seen clearly that the active sites are the broken P sites, which is consistent with our theoretical prediction. B) Comparison of LSV curves for Pt/C, Ni foam, and RuP₄ nanostructures in acid and alkaline conditions. C) Comparison of the TOF values for RuP₄ and state-of-the-art catalysts. D) Relative HER efficiency of the OAIs FeP₄, MoS₂, and FeS₂, and the trivial insulators Fe₂O₃ and FeS (scaled by specific surface areas).

abundant elements. Moreover, we identified FeP₄ as a highly interesting candidate for photocatalytic water splitting, since it has a suitable bandgap of ≈ 1.8 eV, matching the spectra of visible light. We prepared a series of photocatalysts including the OAIs, FeP₄, MoS₂, and FeS₂ (Tables S5 and S6, Supporting Information) as well as the trivial (non-obstructed) insulators Fe₂O₃ and FeS (Figure S16, Supporting Information). The typical temporal evolution of H₂ curves suggests an impressive activity of the synthesized FeP₄ microcrystals (Figure S17, Supporting Information). When scaled by the surface area (Figure S18, Supporting Information), all the OAIs exhibit dramatically better intrinsic activities than normal insulators, as shown in Figure 4D.

3. Conclusion and Outlook

We have demonstrated our concept of identifying novel catalysts using calculations of OSSs with just a few highly promising examples that span stoichiometric compounds with crystal structures ranging from 2D van der Waals to

phosphides. Beyond these examples, we have identified 465 OAIs with promising catalytic activities from among the known 34 013 topologically trivial insulators. The positions of the OSSs for these 465 OAIs are listed in Appendix A in the Supporting Information. Although surface reconstruction and even surface oxidation are inevitable during the catalysis reactions,^[47,48] We believe that OSSs-based descriptor still works in the indentation of active sites. For the OAIs in this work, the localized Wannier functions and electronic states are pinned at the empty sites that do not overlap with the Wyckoff positions of the atoms. This implies the high stability of the OSSs because they are protected by bulk crystal symmetry. Surface reconstruction will certainly influence the apparent activities of the precatalysts,^[49] but will not alter the position of the most active sites as long as the bulk symmetries are not completely broken.^[50,51] However, it should be noted that the theory developed in this work is effective in searching for active sites, but cannot tell the absolute catalytic activity of a given catalyst. The crystal surfaces characterized by OSSs may be too active for catalysis, leading to the strong interaction with the adsorbates and hinders them from catalysis applications. The classic d band theory based

on Sabatier's principle still works for OAI, making sure that the surfaces with OSSs have proper adsorption energy with the reactants such as H, O, and CO.

Most excitingly, a subset of these selected compounds, including the iron-sulfur minerals FeS and FeS₂, exhibit chiral OSSs due to the loss of mirror symmetries at some of their surfaces. Though the compounds have achiral cubic space groups, one can speculate that OSSs on the surfaces of the chiral plane group can be used for the synthesis of chiral molecules.^[52,53] Our work demonstrates that metallic OSSs derived from bulk symmetry calculations are the catalytic activity origin of inorganic heterogeneous catalysts. We conjecture that OSSs can be used for other electrocatalytic reactions beyond HER.

Supporting Information

Supporting Information is available from the Wiley Online Library or from the author.

Acknowledgements

G.L. and Y.X. contributed equally to this work. This work was financially supported by the European Research Council (ERC Advanced Grant No. 742068 "TOPMAT"). The authors also acknowledge funding by the DFG through SFB 1143 (project ID. 247310070) and the Würzburg-Dresden Cluster of Excellence on Complexity and Topology in Quantum Matter ct.qmat (EXC2147, project ID. 39085490) and via DFG project HE 3543/35-1. B.A.B.'s work is part of a project that has received funding from the European Research Council (ERC) under the European Union's Horizon 2020 research and innovation program (grant agreement no. 101020833). U.G. thanks Dr. Guangbo Chen and Prof. Xinliang Feng for measuring the specific surface areas. G.L. thanks the support from the startup foundation of Ningbo Institute of Materials Technology and Engineering (NIMTE), CAS, and the foundation of the director of NIMTE, CAS. G.L. also thanks Prof. Qihong Chen and Dr. Li Xu in the Institute of Physics (IOP), CAS for making the exfoliated MoS₂ nanoflakes.

Open access funding enabled and organized by Projekt DEAL.

Conflict of Interest

The authors declare no conflict of interest.

Data Availability Statement

The data that support the findings of this study are available from the corresponding author upon reasonable request.

Keywords

active sites, catalytic origins, hydrogen evolution, obstructed surface states, Wannier charge centers

Received: February 10, 2022

Revised: April 9, 2022

Published online: May 5, 2022

[1] X. Zhang, M. Zhang, Y. Deng, M. Xu, L. Artiglia, W. Wen, R. Gao, B. Chen, S. Yao, X. Zhang, M. Peng, J. Yan, A. Li, Z. Jiang, X. Gao, S. Cao, C. Yang, A. J. Kropf, J. Shi, J. Xie, M. Bi, J. A. van Bokhoven,

- Y. W. Li, X. Wen, M. Flytzani-Stephanopoulos, C. Shi, W. Zhou, D. Ma, *Nature* **2021**, 589, 396.
- [2] A. Wang, J. Li, T. Zhang, *Nat. Rev. Chem.* **2018**, 2, 65.
- [3] J. Zhang, G. Chen, K. Mullen, X. Feng, *Adv. Mater.* **2018**, 30, 1800528.
- [4] T. F. Jaramillo, K. P. Jorgensen, J. Bonde, J. H. Nielsen, S. Horch, I. Chorkendorff, *Science* **2007**, 317, 100.
- [5] S. Kattel, P. J. Ramírez, J. G. Chen, P. A. Rodriguez, P. Liu, *Science* **2017**, 355, 1296.
- [6] D. Yang, Q. Zhu, B. Han, *Innovation* **2020**, 1, 100016.
- [7] V. Papa, Y. Cao, A. Spannenberg, K. Junge, M. Beller, *Nat. Catal.* **2020**, 3, 135.
- [8] Y. Liu, G. G. Yu, D. Li, Y. Sun, T. Asefa, W. Chen, X. Zou, *Angew. Chem.* **2015**, 54, 10752.
- [9] B. Garlyyev, J. Fichtner, O. Pique, O. Schneider, A. S. Bandarenka, F. Calle-Vallejo, *Chem. Sci.* **2019**, 10, 8060.
- [10] G. Chen, T. Wang, J. Zhang, P. Liu, H. Sun, X. Zhuang, M. Chen, X. Feng, *Adv. Mater.* **2018**, 30, 1706279.
- [11] Z. W. Seh, J. Kibsgaard, C. F. Dickens, I. Chorkendorff, J. K. Norskov, T. F. Jaramillo, *Science* **2017**, 355, eaad4998.
- [12] J. Gao, Y. Qian, H. Jia, Z. Guo, Z. Fang, M. Liu, H. Weng, Z. Wang, *Sci. Bull.* **2021**, 67, 598.
- [13] G. Li, C. Fu, W. Shi, L. Jiao, J. Wu, Q. Yang, R. Saha, M. E. Kammaing, A. K. Srivastava, E. Liu, A. N. Yazdani, N. Kumar, J. Zhang, G. R. Blake, X. Liu, M. Fahlman, S. Wirth, G. Auffermann, J. Gooth, S. Parkin, V. Madhavan, X. Feng, Y. Sun, C. Felser, *Angew. Chem.* **2019**, 58, 13107.
- [14] H. Xie, T. Zhang, R. Xie, Z. Hou, X. Ji, Y. Pang, S. Chen, M. M. Titirici, H. Weng, G. Chai, *Adv. Mater.* **2021**, 33, 2008373.
- [15] Y. He, D. Yan, L. R. Ng, L. Shi, S. Wang, H. Lin, S.-H. Lin, H. Luo, K. Yan, *Mater. Chem. Front.* **2019**, 3, 2184.
- [16] B. Yan, B. Stadtmüller, N. Haag, S. Jakobs, J. Seidel, D. Jungkenn, S. Mathias, M. Cinchetti, M. Aeschlimann, C. Felser, *Nat. Commun.* **2015**, 6, 10167.
- [17] Y. Sun, Y. Zhang, C.-X. Liu, C. Felser, B. Yan, *Phys. Rev. B* **2017**, 95, 235104.
- [18] L. Li, J. Zeng, W. Qin, P. Cui, Z. Zhang, *Nano Energy* **2019**, 58, 40.
- [19] L. Wang, X. Zhang, W. Meng, Y. Liu, X. Dai, G. Liu, *J. Mater. Chem. A* **2021**, 9, 22453.
- [20] Q. Yang, G. Li, K. Manna, F. Fan, C. Felser, Y. Sun, *Adv. Mater.* **2020**, 32, 1908518.
- [21] G. Li, Y. Sun, J. Rao, J. Wu, A. Kumar, Q. N. Xu, C. Fu, E. Liu, G. R. Blake, P. Werner, B. Shao, K. Liu, S. Parkin, X. Liu, M. Fahlman, S.-C. Liou, G. Auffermann, J. Zhang, C. Felser, X. Feng, *Adv. Energy Mater.* **2018**, 8, 1801258.
- [22] Z.-D. Song, L. Elcoro, B. A. Bernevig, *Science* **2020**, 367, 794.
- [23] a) Topological Materials Database, <https://www.topological-quantumchemistry.com/> (accessed: August 2021); b) B. Bradlyn, L. Elcoro, J. Cano, M. G. Vergniory, Z. Wang, C. Felser, M. I. Aroyo, B. A. Bernevig, *Nature* **2017**, 547, 298.
- [24] Y. Xu, L. Elcoro, Z. D. Song, B. J. Wieder, M. G. Vergniory, N. Regnault, Y. Chen, C. Felser, B. A. Bernevig, *Nature* **2020**, 586, 702.
- [25] L. Elcoro, B. J. Wieder, Z. Song, Y. Xu, B. Bradlyn, B. A. Bernevig, *Nat. Commun.* **2021**, 12, 5965.
- [26] Y. Xu, L. Elcoro, G. Li, Z.-D. Song, N. Regnault, Q. Yang, Y. Sun, S. Parkin, C. Felser, B. A. Bernevig arXiv:2111.02433, **2021**.
- [27] G. Bergerhoff, R. Hundt, R. Sievers, I. D. Brown, *J. Chem. Inf. Comput. Sci.* **1983**, 23, 66.
- [28] J. Kibsgaard, Z. Chen, B. N. Reinecke, T. F. Jaramillo, *Nat. Mater.* **2012**, 11, 963.
- [29] J. C. McGlynn, T. Dankwort, L. Kienle, N. A. G. Bandeira, J. P. Fraser, E. K. Gibson, I. Cascallana-Matias, K. Kamaras, M. D. Symes, H. N. Miras, A. Y. Ganin, *Nat. Commun.* **2019**, 10, 4916.
- [30] Y. He, M. Boubeche, Y. Zhou, D. Yan, L. Zeng, X. Wang, K. Yan, H. Luo, *J. Phys.: Mater.* **2020**, 4, 014001.

- [31] H. Li, C. Tsai, A. L. Koh, L. Cai, A. W. Contryman, A. H. Fragapane, J. Zhao, H. S. Han, H. C. Manoharan, F. Abild-Pedersen, J. K. Nørskov, X. Zheng, *Nat. Mater.* **2016**, *15*, 48.
- [32] G. Li, J. Huang, Q. Yang, L. Zhang, Q. Mu, Y. Sun, S. Parkin, K. Chang, C. Felser, *J. Energy Chem.* **2021**, *62*, 516.
- [33] T. A. Ho, C. Bae, S. Lee, M. Kim, J. M. Montero-Moreno, J. H. Park, H. Shin, *Chem. Mater.* **2017**, *29*, 7604.
- [34] Y. Qi, P. G. Naumov, M. N. Ali, C. R. Rajamathi, W. Schnelle, O. Barkalov, M. Hanfland, S. C. Wu, C. Shekhar, Y. Sun, V. Suss, M. Schmidt, U. Schwarz, E. Pippel, P. Werner, R. Hillebrand, T. Forster, E. Kampert, S. Parkin, R. J. Cava, C. Felser, B. Yan, S. A. Medvedev, *Nat. Commun.* **2016**, *7*, 11038.
- [35] S. L. Li, K. Tsukagoshi, E. Orgiu, P. Samori, *Chem. Soc. Rev.* **2016**, *45*, 118.
- [36] Y. Yu, G. H. Nam, Q. He, X. J. Wu, K. Zhang, Z. Yang, J. Chen, Q. Ma, M. Zhao, Z. Liu, F. R. Ran, X. Wang, H. Li, X. Huang, B. Li, Q. Xiong, Q. Zhang, Z. Liu, L. Gu, Y. Du, W. Huang, H. Zhang, *Nat. Chem.* **2018**, *10*, 638.
- [37] J. Wang, X. Li, B. Wei, R. Sun, W. Yu, H. Y. Hoh, H. Xu, J. Li, X. Ge, Z. Chen, C. Su, Z. Wang, *Adv. Funct. Mater.* **2020**, *30*, 1908708.
- [38] Y. Luo, Z. Zhang, F. Yang, J. Li, Z. Liu, W. Ren, S. Zhang, B. Liu, *Energy Environ. Sci.* **2021**, *14*, 4610.
- [39] W. Zhang, D. Li, L. Zhang, X. She, D. Yang, *J. Energy Chem.* **2019**, *39*, 39.
- [40] J. Yu, Y. Guo, S. She, S. Miao, M. Ni, W. Zhou, M. Liu, Z. Shao, *Adv. Mater.* **2018**, *30*, 1800047.
- [41] Z. Pu, I. S. Amiinu, Z. Kou, W. Li, S. Mu, *Angew. Chem., Int. Ed.* **2017**, *56*, 11559.
- [42] H. B. Zhang, P. F. An, W. Zhou, B. Y. Guan, P. Zhang, J. C. Dong, X. W. Lou, *Sci. Adv.* **2018**, *4*, aao6657.
- [43] Y. Liu, S. Liu, Y. Wang, Q. Zhang, L. Gu, S. Zhao, D. Xu, Y. Li, J. Bao, Z. Dai, *J. Am. Chem. Soc.* **2018**, *140*, 2731.
- [44] Y. Li, F. Chu, Y. Liu, Y. Kong, Y. Tao, Y. Li, Y. Qin, *Chem. Commun.* **2018**, *54*, 13076.
- [45] Q. Xu, G. Li, Y. Zhang, Q. Yang, Y. Sun, C. Felser, *ACS Catal.* **2020**, *10*, 5042.
- [46] Y. Yuan, S. Adimi, T. Thomas, J. Wang, H. Guo, J. Chen, J. P. Attfield, F. J. DiSalvo, M. Yang, *Innovation* **2021**, *2*, 100096.
- [47] J. Wang, S.-J. Kim, J. Liu, Y. Gao, S. Choi, J. Han, H. Shin, S. Jo, J. Kim, F. Ciucci, H. Kim, Q. Li, W. Yang, X. Long, S. Yang, S.-P. Cho, K. H. Chae, M. G. Kim, H. Kim, J. Lim, *Nat. Catal.* **2021**, *4*, 212.
- [48] J. Wang, Y. Gao, H. Kong, J. Kim, S. Choi, F. Ciucci, Y. Hao, S. Yang, Z. Shao, J. Lim, *Chem. Soc. Rev.* **2020**, *49*, 9154.
- [49] Y. Duan, S. Sun, Y. Sun, S. Xi, X. Chi, Q. Zhang, X. Ren, J. Wang, S. J. H. Ong, Y. Du, L. Gu, A. Grimaud, Z. J. Xu, *Adv. Mater.* **2019**, *31*, 1807898.
- [50] Y. Zhang, L. Gao, E. J. M. Hensen, J. P. Hofmann, *ACS Energy Lett.* **2018**, *3*, 1360.
- [51] G. Li, S. Khim, C. S. Chang, C. Fu, N. Nandi, F. Li, Q. Yang, G. R. Blake, S. Parkin, G. Auffermann, Y. Sun, D. A. Muller, A. P. Mackenzie, C. Felser, *ACS Energy Lett.* **2019**, *4*, 2185.
- [52] Y. Liu, J. Xiao, J. Koo, B. Yan, *Nat. Mater.* **2021**, *20*, 638.
- [53] R. Naaman, Y. Paltiel, D. H. Waldeck, *Nat. Rev. Chem.* **2019**, *3*, 250.